A broad-spectrum virus- and host-targeting antiviral peptide against SARS-CoV-2 and other respiratory viruses

Hanjun Zhao
State Key Laboratory of Emerging Infectious Diseases and and Department of Microbiology, Li Ka Shing Faculty of Medicine, The University of Hong Kong

Kelvin K. W. To
State Key Laboratory of Emerging Infectious Diseases and and Department of Microbiology and Carol Yu Centre for Infection, Li Ka Shing Faculty of Medicine, The University of Hong Kong

Kong-Hung Sze
State Key Laboratory of Emerging Infectious Diseases and and Department of Microbiology, Li Ka Shing Faculty of Medicine, The University of Hong Kong

Timothy Tin-Mong Yung
State Key Laboratory of Emerging Infectious Diseases, Li Ka Shing Faculty of Medicine, The University of Hong Kong

Mingjie Bian
School of Life Science, Anhui Normal University

Hoiyan Lam
State Key Laboratory of Emerging Infectious Diseases, Li Ka Shing Faculty of Medicine, The University of Hong Kong

Cun Li
State Key Laboratory of Emerging Infectious Diseases, Li Ka Shing Faculty of Medicine, The University of Hong Kong

Hin Chu
State Key Laboratory of Emerging Infectious Diseases and and Department of Microbiology, Li Ka Shing Faculty of Medicine, The University of Hong Kong

Kwok-Yung Yuen (✉ kyyuen@hku.hk)
State Key Laboratory of Emerging Infectious Diseases and and Department of Microbiology and Carol Yu Centre for Infection, Li Ka Shing Faculty of Medicine, The University of Hong Kong

---

Research Article

Keywords: defensin-like peptide, P9R, antiviral activity, pH-dependent viruses, SARS-CoV-2, SARS-CoV, MERS-CoV, pandemic A(H1N1)pdm09 virus, avian influenza A(H7N9) virus, non-enveloped rhinovirus

Posted Date: March 20th, 2020

DOI: https://doi.org/10.21203/rs.3.rs-18687/v1

Version of Record: A version of this preprint was published on August 25th, 2020. See the published version at https://doi.org/10.1038/s41467-020-17986-9.

Abstract

The 2019 novel respiratory virus (SARS-CoV-2) causes COVID-19 with rapid global socioeconomic disruptions and disease burden to healthcare. The current COVID-19 and previous emerging virus outbreaks highlight the urgent need for broad-spectrum antivirals. Here, we showed that a defensin-like peptide P9R exhibited potent antiviral activity against pH-dependent viruses that require endosomal acidification for virus-host membrane fusion, including the enveloped coronaviruses (SARS-CoV-2, SARS-CoV and MERS-CoV), the pandemic A(H1N1)pdm09 virus, avian influenza A(H7N9) virus, and the non-enveloped rhinovirus. P9R could significantly protect mice from lethal challenge by A(H1N1)pdm09 virus and showed low possibility to cause drug-resistance virus. Mechanistic studies indicated that the antiviral activity of P9R depended on the direct binding to viruses and the inhibition of virus-host endosomal acidification, which provides a new concept that virus-binding alkaline peptides could broadly inhibit pH-dependent viruses. These results suggest that the dual-functional virus- and host-targeting P9R could be a promising candidate for combating pH-dependent respiratory viruses.

Authors Hanjun Zhao, Kelvin K. W. To, and Kong-Hung Sze contributed equally to this work.

Introduction

Novel respiratory viruses often cause severe respiratory tract infections and spread quickly due to the lack of pre-existing immunity. In the recent two decades, three highly pathogenic coronaviruses have crossed species barrier and caused human diseases, including the bat-related severe acute respiratory syndrome coronavirus (SARS-CoV) in 2003[1, 2], the Middle East respiratory syndrome coronavirus (MERS-CoV) since 2012[3, 4] and the recent 2019 new coronavirus (SARS-CoV–2)[5]. Furthermore, the 2009 pandemic influenza A(H1N1)pdm09 virus had led to the 1st influenza pandemic in the 21st century, and the avian influenza virus A(H7N9) had caused a large zoonotic outbreak in mainland China[6, 7]. Due to the lack of effective antivirals, especially for coronaviruses, these respiratory viruses are associated with significant morbidity and mortality. Furthermore, these emerging respiratory viruses have also caused severe economic and social disturbances.

The COVID–2019 outbreak has clearly illustrated the importance of broad-spectrum antivirals. While an outbreak of unusual pneumonia was reported from Wuhan of China in December 2019, the identity of SARS-CoV–2 was reported on January 8, 2020 by China CDC[8]. Currently, there is no specific drug treatment for this new virus. An effective broad-spectrum antiviral will improve patients' outcome and may reduce transmission in the community and hospitals even before the identification of the novel emerging virus and the specific antiviral drug.

In past decades, researchers and our group have devoted to the discovery of broad-spectrum antivirals targeting hosts or viruses[9, 10]. Most broad-spectrum antivirals are targeting host pathways which are utilized by many viruses in their life cycles for viral replication or by stimulating host antiviral immunity[11, 12]. We have previously reported a broad-spectrum antiviral peptide P9[13]. This peptide, derived from

mouse β-defensin–4, was found to have antiviral activity against SARS-CoV, MERS-CoV, and influenza viruses by inhibiting endosomal acidification. We have also reported antiviral peptides against influenza virus by delivering defective interfering gene[14], zika virus by targeting envelope protein[15], MERS-CoV by blocking viral fusion[16]. Other groups have reported the broad-spectrum antiviral peptide BanLec inhibiting HIV, hepatitis C virus (HCV) and influenza virus[17], retrocyline 2 inhibiting influenza virus, Sindbis virus, and baculovirus[18], mastoparan inhibiting enveloped viruses[19], mucroporin-M1 inhibiting measles, SARS-CoV and H5N1 virus[20], Ev37 inhibiting dengue virus, HCV, zika virus, and herpes simples virus[21], and other host defense peptides inhibiting different enveloped and no-enveloped viruses with documented or unknown mechanism[22–24]. Since the first anti-HIV peptide enfuvirtide was approved by FDA for the treatment of HIV in 2003[25], other peptides with antiviral activity have been approved by FDA[26].

Here, we reported a potent antiviral peptide P9R, derived from mouse β-defensin–4 and our previous P9[13], which exhibited very broad-spectrum antiviral activities against the enveloped SARS- CoV–2, MERS-CoV, SARS-CoV, A(H1N1)pdm09, A(H7N9) virus, and the non-enveloped rhinovirus. *In vivo* study indicated that P9R could efficiently protect mice from lethal A(H1N1)pdm09 virus challenge. Furthermore, the antiviral resistance study indicated that P9R did not cause emergency of drug-resistant virus even after A(H1N1)pdm09 virus was passaged in the presence of P9R for 40 passages. Mechanistic studies showed that positively charged P9R broadly inhibits viral replication by binding to different viruses and then inhibiting virus-host endosomal acidification to prevent the endosomal release of pH-dependent viruses. We used P9R (not only binding to viruses but also inhibiting endosomal acidification), PA1 (only binding to viruses) and P9RS (only inhibiting endosomal acidification) to identify and confirm the novel antiviral mechanism of alkaline peptides. The antiviral activity of alkaline peptide could be enhanced by increasing the positive charge of peptide and required both of binding to viruses and inhibiting endosomal acidification.

Results

Mouse Beta-defensin-derived peptide P9R could broadly inhibit coronaviruses and other respiratory viruses

Endosomal acidification is affected by the influx of protons into the endosome via the vacuolar membrane proton pump V-ATPase[27]. Theoretically, an alkaline peptide with stronger net positive charge would neutralize protons in the endosome, thereby inhibiting the endosomal acidification. Hence, to improve our previously antiviral peptide P9[13], we substituted the weakly positively charged amino acids (histidine and lysine) by arginine at positions 21 (H→R), 23 (K→ R) and 28 (K→R) (Fig. 1a) to increase the net positive charge (+4.7) of P9 to charge (+5.6) of P9R. In the plaque reduction assay, the IC_{50} of P9R against SARS-CoV–2 was significantly lower than that of P9 (0.9 μg ml^{-1} vs 2.4 μg ml^{-1}, $P<0.01$) (Fig. 1b). Furthermore, P9R showed significantly stronger inhibition against MERS- CoV, A(H1N1)pdm09 virus, A(H7N9) virus, and rhinovirus than P9 (Fig. 1c–1g). However, the IC_{50} of P9R and P9 against

parainfluenza virus 3 was much higher (>25.0 μg ml^{-1}), likely because endosomal acidification was not required in the viral life cycle of parainfluenza virus 3 (Fig. 1h)[28]. In the multicycle growth assay, P9R inhibited viral replication by 1000-fold for SARS-CoV–2, MERS- CoV, and SARS-CoV (Fig. 1i). For A(H1N1)pdm09 virus, A(H7N9) virus and rhinovirus, P9R could inhibit >20-fold viral replication (Fig. 1i). In addition, the CC_{50} of P9R was >300 μg ml^{-1} for MDCK, VeroE6 and A549 cells (Fig. 1j). These results indicated that P9R with more positive charge could more efficiently inhibit the new coronavirus SARS-CoV–2 and other enveloped and non-enveloped respiratory viruses than that of P9.

The degree of positive charge is critical for the inhibition of endosomal acidification and antiviral activity

To determine whether the net charge of the peptide affects the inhibition of endosomal acidification, using the endosomal acidification assay, we identified that P9R (+5.6) could more significantly inhibit endosomal acidification in live cells than that of P9 (Fig. 2ab), which are consistent with the stronger antiviral activity of P9R than that of P9. In addition, peptide PA1 with less positive charge (+1.7), which has the same amino acid sequence as P9 except 3 additional acidic amino acid at the C terminal, could not inhibit endosomal acidification (Fig. 2ab) and lost the antiviral activity (Fig. 2c). Hence, the degree of net positive charge was correlated with the degree of inhibition of endosomal acidification and antiviral activity.

Inhibition of host endosomal acidification alone is not sufficient for positively charged peptide inhibiting virus replication

To determine whether the antiviral activity solely relied on the positive charge of peptide, we designed a peptide P9RS (+5.6) which had the same positive charge as P9R (+5.6), but P9RS differed from P9R by 11 of 30 amino acids. P9RS efficiently inhibited host endosomal acidification to the similar degree as P9R in live cells (Fig. 2ab). However, in the plaque reduction assay, there was no significant reduction of plaque numbers for SARS-CoV–2 and A(H1N1)pdm09 virus when viruses were treated by P9RS even at 25 μg ml^{-1} (Fig. 2c).

To investigate why P9RS failed to inhibit viral replication despite potent inhibition of host endosomal acidification, we studied the binding between the peptide and virus. Using ELISA-RT- qPCR assay, P9R and PA1 could efficiently bind to SARS-CoV–2 and A(H1N1)pdm09 virus but P9RS did not bind to SARS-CoV–2 and A(H1N1)pdm09 virus (Fig. 2d). The observation of P9R but not P9RS binding to virus was further confirmed by confocal microscopy in H1N1-infected cells (Fig. 2e). Thus, the direct interaction of peptide with virus was required for the antiviral activity of positively charged peptide P9R. In contrast, P9RS

without the ability of binding to virus could not inhibit viral replication even though it carries the same positive charge as P9R and inhibits host endosomal acidification.

The broad-spectrum antiviral activity of P9R relies on targeting viruses to inhibit virus-host endosome acidification

In the above experiments, we had demonstrated that P9R and P9RS can inhibit no-virus endosomal acidification (Fig. 2ab). However, without binding to virus, P9RS could not inhibit viral replication. To illustrate this result, we showed that P9R and bafilomycin A1 could efficiently inhibit the virus-host endosomal acidification in infected live cells, but P9RS could not inhibit the virus-host endosomal acidification in infected live cells (Fig. 3a), even though both of P9R and P9RS could inhibit the endosomal acidification of no-virus endosomes (Fig. 2a). The efficient inhibition of P9R on virus-host endosomal acidification could be due to the binding of P9R to virus (Fig. 2de) and then inhibiting the virus-host endosomal acidification (Fig. 3a). Lacking the binding ability to viruses (Fig. 2de), P9RS could not efficiently enter endosomes with the viruses to inhibit the virus-host endosomal acidification, possibly because the presence of virus in endosomes prevented the entry of unbonded P9RS into the endosomes. Without viruses in endosomes, there were empty spaces in no-virus endosomes to allow P9RS freely entering endosomes to prevent endosomal acidification (Fig. 2a). It should be noted that PA1 with a similar sequence as P9R could efficiently bind to SARS-CoV–2 and A(H1N1)pdm09 virus (Fig. 2d), but it significantly lost the antiviral activity against SARS-CoV–2 and A(H1N1)pdm09 virus (Fig. 2c). The binding of P9R to SARS-CoV–2 and A(H1N1)pdm09 virus could be significantly reduced when viruses were pretreated by PA1 (Fig. 3b). This indicated that PA1 had the same binding sites on viral particles as P9R but only peptide binding to virus alone could not account for the antiviral activity. P9R binding to virus was the first step to exert the antiviral activity.

After binding to virus (Fig. 2e), P9R could efficiently inhibit virus-host endosomal acidification (Fig. 3a) and then inhibit viral replication by blocking RNP release (Fig. 3c).

To further confirm that broad-spectrum antiviral activity of P9R was due to the broadly bindings of P9R to different viruses and viral proteins, we demonstrated that P9R but not P9RS could also bind to MERS-CoV, A(H7N9) virus, rhinovirus, SARS-CoV and viral proteins (Fig. 3d–3f and Fig. S1). This result further confirmed that positively charged P9R could inhibit pH-dependent endosomal viruses if it can bind to viruses.

Next, we tried to determine the structure of P9R using NMR spectroscopy. The results indicated that the solution structure of P9R was flexible with short variable helical patches and with positively charged peptide surface (Fig. 3g). We hypothesized that P9R could broadly bind to different viruses because these

short α-helical patches with flexible linkages may allow it to adapt its structure to fit the binding pockets of different viral proteins. More co-binding structure analysis will be needed for identifying the broadly binding mechanism of P9R with different viral proteins in future. In conclusion, here we demonstrated the novel antiviral mechanism that positively charged P9R needs targeting viruses and then prevents virus-host endosomal acidification to inhibit pH-dependent virus replication. *The efficacy of P9R treatment in vivo*

We had demonstrated that the efficient antiviral activity of P9R *in vitro* is reliant on binding to viruses and the positive charge of P9R to inhibit virus-host endosomal acidification. To further investigate the antiviral activity of P9R *in vivo,* we treated A(H1N1)pdm09-infected mice at 6 h post infection with additional two doses in the following one day. In this model, 80% of P9R-treated mice survived, which was significantly better than PBS-treated group and PA1-treated group (Fig. 4a). The protection of P9R on infected mice was the same as that in the zanamivir-treated group (80%) and was better than P9. From day 4 to day 10 post infection, there was significantly less body weight loss in P9R group than that in PBS-treated group and PA1-treated group (Fig. 4b). The low dose protection of P9R (25 μg/dose and 12.5 μg/dose) on infected mice and reducing body weight loss further demonstrated that P9R could significantly protect mice when compared with PBS-treated group (Fig. 4cd). The antiviral activity of P9R *in vivo* was better than that of P9 (Fig. 4c, P<0.05 for 12.5μg/dose), which was consistent with the significantly better antiviral activity of P9R than P9 *in vitro.*

No emergence of resistant viruses against P9R after serial passages of virus in the presence of P9R

Emergence of resistant mutants occur from time to time[14], especially with the new polymerase inhibitor baloxavir[29]. To determine whether P9R treatment induces viral resistance, A(H1N1)pdm09 virus was serially passaged 40 times in the presence of P9R in MDCK cells (Fig. 5a). A(H1N1)pdm09 virus was serially passaged in the presence of zanamivir as a control for resistance assay (Fig. 5a). The IC_{50} of zanamivir against parent A(H1N1)pdm09 virus (P0) was 35 nM (Fig. 5b). After 10-virus passages in the presence of zanamivir (100 nM) and additional 5-virus passages in the presence of zanamivir (1000 nM), 2000 nM and 8000 nM zanamivir could not inhibit P10 and P15 virus replication, respectively (Fig. 5c). These indicated that after 10 passages of virus in the presence of zanamivir had caused significant viral resistance to zanamivir. However, for P9R, even the A(H1N1)pdm09 virus was passaged in the presence (5.0 μg ml^{-1} of P9R for the initial 10 passages and 50.0 μg ml^{-1} for the rest 30 passages) of P9R for 40 passages, P9R (5.0 μg ml^{-1}) could efficiently inhibit P30 and P40 virus replication (Fig. 5d). No obvious drug-resistant virus to P9R was detected. These results indicated that P9R had very low possibility to cause drug-resistant virus.

Discussion

In this study, we identified a broad-spectrum antiviral peptide P9R with potent antiviral activity against enveloped coronaviruses (SARS-CoV–2, SARS-CoV and MERS-CoV), influenza virus, and non-enveloped rhinovirus. First, we demonstrated that the antiviral activity of P9R could be significantly enhanced by increasing the net positive charge to more efficiently inhibit endosomal acidification. Second, mechanistic studies further demonstrated the novel antiviral mechanism that positively charged P9R could bind to different respiratory viruses to inhibit virus-host endosomal acidification. PA1 (only binding to viruses) or P9RS (only inhibiting endosomal acidification) did not show antiviral activity. Third, the *in vivo* antiviral activity of P9R was demonstrated by protecting mice from lethal influenza virus challenge. Fourth, there was no reduced susceptibility of serial-passaged viruses (40 passages) against P9R.

The 'one bug-one drug' approach to antiviral drug is successful for HIV, hepatitis C virus and influenza virus[9]. However, there is an urgent need for broad-spectrum antivirals for combating emerging and re-emerging new virus outbreaks, such as the SARS-CoV–2, before the new virus is identified or specific antiviral drug is available.

Endosomal acidification is a key step in the life cycle of many pH-dependent viruses, which is one of the broad-spectrum antiviral targets[9]. In this study, with the increased positive charge in P9R, it could more efficiently inhibit pH-dependent viruses than that of P9. The more positive charge in P9R allowed the peptide to more efficiently neutralize protons inside endosomes, and thereby inhibiting the endosomal acidification. In previous studies, the clinically approved anti-malarial drug chloroquine with activity of inhibiting endosomal acidification had been demonstrated to inhibit enterovirus-A7[30], zika virus[31] and SARS-CoV–2[32]. The anti-parasitic drug niclosamide also inhibited influenza virus, rhinovirus, and dengue virus by interfering endosomal acidification[33, 34]. However, researchers demonstrated the lack of protection of chloroquine *in vivo* for treating influence virus and Ebola virus[35, 36]. Differing from these drugs by interfering host endosomal acidification without targeting viruses, P9R inhibits viral replication by binding to viruses and then inhibiting virus-host endosomal acidification, which allows P9R to selectively and efficiently inhibit endosomal viruses. The protection of P9R on A(H1N1)-infected mice further confirmed the antiviral efficiency *in vivo.*

The antiviral activity of P9R required both of binding to viruses and inhibiting endosomal acidification. PA1 with less positive charge could not inhibit SARS-CoV–2 and H1N1 virus even thought it had the similar binding ability and binding sites to viruses as P9R (Fig. 3b). When we made multiple substitutions on P9R to generate P9RS, P9RS lost the binding ability and antiviral activity to all tested viruses even though P9RS had the same positive charge as P9R and efficiently inhibited host endosomal acidification. The broadly binding mechanism of P9R to different viral proteins may be due to the flexible structure of P9R with positively charged surface (Fig. 3h). The flexible structure may allow P9R to change its structure to fit targeting proteins for broad-specificity bindings[37, 38], and the positive charge of P9R may play roles for binding to viruses with negatively charged surface[39, 40]. The five cysteines in P9R may also affect the structure-based binding because previous studies indicated that cysteine substitutions could affect defensin-peptide structure and activity[41, 42].

In addition, comparing with zanamivir which caused significant drug resistance virus after 10- virus passages in the presence of zanamivir, P9R showed very low risk to cause drug-resistance virus even A(H1N1)pdm09 virus was passaged in the presence of P9R for 40 passages. The low risk of resistance induction by P9R may be partially due to the dual targeting ability to broadly bind to viruses and target host endosomes. More co-binding structure analysis will be needed to illustrate the broadly binding mechanism and help to understand the low drug resistance mechanism in future study.

In summary, most highly pathogenic emerging viruses are endosomal pH-dependent viruses. The emerging and re-emerging virus outbreaks remind us of the urgent need of broad-spectrum antivirals. Continual studies on this kind of antivirals, which can broadly bind to different viruses and inhibit pH-dependent viruses by preventing virus-host endosomal acidification with low possibility of causing drug resistance, will give us more armamentarium to combat novel emerging virus outbreaks in future.

Material And Methods

Cells and virus culture

Madin Darby canine kidney (MDCK, CCL–34), Vero E6 (CRL–1586), RD (CCL136), LLC- MK2 (CCL–7), A549 (CCL–185) cells obtained from ATCC (Manassas, VA, USA) were cultured in Dulbecco minimal essential medium (DMEM) or MEM supplemented with 10% fetal bovine serum (FBS), 100 IU ml^{-1} penicillin and 100 μg ml^{-1} streptomycin. The virus strains used in this study included 2019 new coronavirus (SARS-CoV–2)[43], SARS-CoV, MERS-CoV (hCoV-EMC/2012), A/Hong Kong/415742/2009, A/Hong Kong/415742Md/2009 (H1N1) (a highly virulent mouse-adapted strain), A/Anhui/1/2013 (H7N9)[13], rhinovirus[44] and human parainfluenza 3 (ATCC-C243). For in vitro experiments, viruses were cultured in MDCK, Vero E6, RD and LLC-MK2 cells. For animal experiments, H1N1 virus was cultured in eggs as described previously[45].

Design and synthesis of peptides

P9, P9R, PA1 and P9RS were designed as shown in Fig. 1a and synthesized by ChinaPeptide (Shanghai, China). The purity of all peptides was>95%. The purity and mass of each peptide were verified by HPLC and mass spectrometry.

Plaque reduction assay

Antiviral activity of peptides was measured using a plaque reduction assay as we described previously[14]. Briefly, peptides were dissolved in 30 mM phosphate buffer containing 24.6 mM Na_2HPO_4 and 5.6 mM KH_2PO_4 at a pH of 7.4. Peptides or bovine serum albumin (BSA, 0.4–50.0 μg ml^{-1}) were premixed with 50 PFU of coronaviruses (SARS-CoV–2, MERS-CoV, and SARS-CoV), influenza viruses (H1N1 virus and H7N9

virus), rhinovirus, or parainfluenza 3 in phosphate buffer at room temperature. After 1 h of incubation, peptide-virus mixture was transferred to Vero E6 for coronaviruses, MDCK for influenza viruses, RD for rhinoviruses, or LLC-MK2 for parainfluenza virus. At 1 h post infection, infectious media were removed and 1% low melting agar was added to cells. Cells were fixed using 4% formalin at 2–4 day post infection. Crystal blue (0.1%) was added for staining, and the number of plaques was counted.

Antiviral multicycle growth assay

Coronaviruses (SARS-CoV–2, MERS-CoV, and SARS-CoV), influenza viruses (H1N1 and H7N9 virus) and rhinovirus (0.005 MOI) were premixed with P9R or BSA (50–100 μg ml^{-1}) in phosphate buffer for 1 h. After incubation, coronaviruses were inoculated onto Vero E6. Influenza viruses were inoculated onto MDCK cells. Rhinovirus was inoculated onto RD cells. After 1h infection, infectious media were removed and fresh media with supplemented P9R or BSA (50–100 μg ml^{-1}) were added to infected cells for virus and cell culture. At 24–30h post infection, the supernatants of cells were collected for detecting viral RNA copies.

Cytotoxicity assay

Cytotoxicity of peptides was determined by the detection of 50% cytotoxic concentration (CC_{50}) using a tetrazolium-based colorimetric MTT assay as we described previously[13]. Briefly, cells were seeded in 96-well cell culture plate at an initial density of 2×10^4 cells per well in MEM or DMEM supplemented with 10% FBS and incubated for overnight. Cell culture media were removed and then DMEM supplemented with various concentrations of peptides and 1% FBS were added to each well. After 24 h incubation at 37 °C, MTT solution (5 mg ml^{-1}, 10 μl per well) was added to each well for incubation at 37 °C for 4 h. Then, 100 μl of 10% SDS in 0.01M HCl was added to each well. After further incubation at room temperature with shaking overnight, the plates were read at OD570 using VictorTM X3 Multilabel Reader (PerkinElmer, USA). Cell culture wells without peptides were used as the experiment control and medium only served as a blank control.

Peptide-virus binding assay

Peptides (0.1 μg per well) dissolved in H_2O were coated onto ELISA plates and incubated at 4 °C overnight. Then, 2% BSA was used to block plates at 4°C overnight. For virus binding to peptides, viruses were diluted in phosphate buffer and then were added to ELISA plate for binding to the coated peptides at room temperature for 1h. After washing the unbinding viruses, the binding viruses were lysed by RLT buffer of RNeasy Mini Kit (Qiagen, Cat# 74106) for viral RNA extraction. Viral RNA copies of binding viruses were measured by RT-qPCR.

ELISA assay

ELISA assay was done as described previously[14]. Peptides (0.1 μg per well) dissolved in H_2O were coated onto ELISA plates and incubated at 4 °C overnight. Then, 2% BSA was used to block plates at 4 °C overnight. For HA and S binding, 150 ng HA1 or S in solution I buffer (Sino Biological Inc., Cat# 11055-V08H4) was incubated with peptides at 37 °C for 1 h. The binding abilities of peptides to HA1 or S proteins were determined by incubation with rabbit anti-His-HRP (Invitrogen, Cat# R93125, 1: 2,000) at room temperature for 30 min. The reaction was developed by adding 50 μl of TMB single solution (Life Technologies, Cat# 002023) for 15 min at 37 °C and stopped with 50 μl of 1 M H_2SO_4. Readings were obtained in an ELISA plate reader (Victor 1420 Multilabel Counter; PerkinElmer) at 450 nm.

Viral RNA extraction and RT-qPCR

Viral RNA was extracted by Viral RNA Mini Kit (QIAGEN, Cat# 52906, USA) according to the manufacturer's instructions. Real-time RT-qPCR was performed as we described previously[14]. Extracted RNA was reverse transcribed to cDNA using PrimeScript II 1st Strand cDNA synthesis Kit (Takara, Cat# 6210A) using GeneAmp® PCR system 9700 (Applied Biosystems, USA). The cDNA was then amplified using specific primers (Table S1) for detecting SARS-CoV–2, MERS-CoV, SARS- CoV, H1N1, H7N9, and rhinovirus using LightCycle® 480 SYBR Green I Master (Roach, USA). For quantitation, 10-fold serial dilutions of standard plasmid equivalent to 10^1 to 10^6 copies per reaction were prepared to generate the calibration curve. Real-time qPCR experiments were performed using LightCycler® 96 system (Roche, USA).

Endosomal acidification assay

Endosomal acidification was detected with a pH-sensitive dye (pHrodo Red dextran, Invitrogen, Cat#P10361) according to the manufacturer's instructions as previously described but with slight modification[14]. First, MDCK cells were treated with BSA (25.0 μg ml^{-1}), P9 (25.0 μg ml^{-1}), P9R (25.0 μg ml^{-1}), PA1 (25.0 μg ml^{-1}), or P9RS (25.0 μgml^{-1}) at 4 °C for 15 min. Second, MDCK cells were added with 100 μg ml^{-1} of pH-sensitive dye and DAPI and then incubated at 4 °C for 15 min. Before taking images, cells were further incubated at 37 °C for 15 min and then cells were washed twice with PBS. Finally, PBS was added to cells and images were taken immediately with confocal microscope (Carl Zeiss LSM 700, Germany).

Colocalization assay of peptide binding to virus in cells

H1N1 virus was labeled by green Dio dye (Invitrogen, Cat#3898) according to the manufacture introduction. DIO-labeled virus was treated by TAMRA-labeled P9R and TAMRA-labeled P9RS for 1h at room temperature. Pre-cool MDCK cells were infected by the peptide-treated virus on ice for 15 min and

then moved to 37 for incubation for 15 min. Cells were washed twice by PBS and then fixed by 4% formalin for 1h. Nuclei were stained by DAPI for taking images by confocal microscope (Carl Zeiss LSM 700, Germany).

Nucleoprotein (NP) immunofluorescence assay.

NP staining was carried out as described previously[14]. MDCK cells were seeded on cell culture slides and were infected with A(H1N1)pdm09 virus at 1 MOI pretreated with BSA (25.0 μg ml^{-1}), bafilomycin A1 (50.0 nM) or P9R (25.0 μg ml^{-1}). After 3.5 h post infection, cells were fixed with 4% formalin for 1 h and then permeabilized with 0.2 % Triton X–100 in PBS for 5 min. Cells were washed by PBS and then blocked by 5% BSA at room temperature for 1 h. Cells were incubated with mouse IgG anti-NP (Millipore, Cat# 2817019, 1:600) at room temperature for 1 h and then washed by PBS for next incubation with goat anti-mouse IgG Alexa–488 (Life Technologies, Cat# 1752514, 1:600) at room temperature for 1 h. Finally, cells were washed by PBS and stained with DAPI. Images were taken by confocal microscope (Carl Zeiss LSM 700, Germany).

NMR Structure analysis of P9R

Freshly prepared 1 mg ml^{-1} (0.29 mM) of P9R in 0.5 ml solvent was used for the NMR study. Data were collected in H_2O/D_2O (19:1 v/v), as well as 99.996% D_2O, with the internal reference trimethylsilylpropanoic acid. All NMR spectra were acquired on either a Bruker AVANCE III 600 MHz spectrometer (Bruker BioSpin, Germany) or a Bruker AVANCE III 700 MHz spectrometer at 25˚C. 2D $^1H–^1H$ correlation spectroscopy (COSY), total correlated spectroscopy (TOCSY) and nuclear Overhauser effect spectroscopy (NOESY) spectra were recorded for resonance assignments. Inter- proton distance restraints were derived from 2D NOESY spectrum with mixing times of 300 ms and 500 ms using automated NOE assignment strategy followed by a manual check. NOE intensities and chemical shifts were extracted using CCPNMR Analysis 2.4.2[46] and served as inputs for the Aria program. Dihedral angle is predicted from the chemical shifts using the program DANGLE[47]. The NMR solution structure of P9R was calculated iteratively using Aria 2.3 program[48]. One hundred random conformers were annealed using distance restraints in each of the eight iteratively cycles of the combined automated NOE assignments and structure calculation algorithm. The final upper limit distance constraints output from the last iteration cycle were subjected to a thorough manual cross- checking and final water solvent structural refinement cycle. The 10 lowest energy conformers were retained from these refined 100 structures for statistical analysis. The convergence of the calculated structures was evaluated using root-mean-square deviations (RMSDs) analyses. The distributions of the backbone dihedral angles (φ, ψ) of the final converged structures were evaluated by representation of the Ramachandran dihedral pattern using PROCHECK-NMR[49]. Visualization of three-dimensional structures and electrostatic surface potential of P9R were achieved using UCSF Chimera 1.13.1[50].

Antiviral analysis of P9R in mice

BALB/c female mice, 10–12 weeks old, were kept in biosafety level 2 laboratory and given access to standard pellet feed and water *ad libitum.* All experimental protocols followed the standard operating procedures of the approved biosafety level 2 animal facilities and were approved by the Committee on the Use of Live Animals in Teaching and Research of the University of Hong Kong[45]. The mouse adapted H1N1 virus was used for lethal challenge of mice. To evaluate the therapeutic effect, mice were challenged with 3 LD_{50} of the virus and then intranasally inoculated with PBS, P9, P9R, PA1 or zanamivir at six hours after the viral inoculation. Two more doses were given to H1N1- challenged mice at the following one day. Survival and general conditions were monitored for 16 days or until death.

Statistical analysis

Survival of mice and the statistical significance were analyzed by GraphPad Prism 5. The statistical significance of the other results was calculated by the two-tailed Student *t* test using Stata statistical software. Results were considered significant at $P < 0.05$.

Declarations

Acknowledgements

This work was supported by donations of Shaw Foundation Hong Kong, Richard Yu and Carol Yu, Michael Seak-Kan Tong, The Respiratory Viral Research Foundation Limited, The Hui Ming, Hui Hoy and Chow Sin Lan, Charity Fund Limited, and funding from Health@InnoHK.

Conflict of interest

The authors declare that they have no conflict of interest.

Data availability.

All data that support the conclusions of the study are available from the corresponding author upon request.

References

1. Woo, P.C. et al. Relative rates of non-pneumonic SARS coronavirus infection and SARS coronavirus pneumonia. *Lancet* **363**, 841-845 (2004).

2. Lau, K. et al. Severe acute respiratory syndrome coronavirus-like virus in Chinese horseshoe bats. *Proc Natl Acad Sci U S A* **102**, 14040-14045 (2005).
3. Chan, J.F. et al. Middle East respiratory syndrome coronavirus: another zoonotic betacoronavirus causing SARS-like disease. *Clinical microbiology reviews* **28**, 465-522 (2015).
4. Yeung, M.L. et al. MERS coronavirus induces apoptosis in kidney and lung by upregulating Smad7 and FGF2. *Nat Microbiol* **1**, 16004 (2016).
5. Chan, J.F. et al. A familial cluster of pneumonia associated with the 2019 novel coronavirus indicating person-to-person transmission: a study of a family cluster. *Lancet* **395**, 514-523 (2020).
6. To, K.K., Chan, J.F., Chen, H., Li, L. & Yuen, K.Y. The emergence of influenza A H7N9 in human beings 16 years after influenza A H5N1: a tale of two cities. *Lancet Infect Dis* **13**, 809-821 (2013).
7. Cheng, V.C., To, K.K., Tse, H., Hung, I.F. & Yuen, K.Y. Two years after pandemic influenza A/2009/H1N1: what have we learned? *Clinical microbiology reviews* **25**, 223-263 (2012).
8. Li, Q. et al. Early Transmission Dynamics in Wuhan, China, of Novel Coronavirus-Infected Pneumonia. *N Engl J Med* (2020).
9. Vigant, F., Santos, N.C. & Lee, B. Broad-spectrum antivirals against viral fusion. *Nat Rev Microbiol* **13**, 426-437 (2015).
10. Yuan, S. et al. SREBP-dependent lipidomic reprogramming as a broad-spectrum antiviral target. *Nat Commun* **10**, 120 (2019).
11. Rajendran, , Knolker, H.J. & Simons, K. Subcellular targeting strategies for drug design and delivery. *Nat Rev Drug Discov* **9**, 29-42 (2010).
12. Yan, N. & Chen, Z.J. Intrinsic antiviral immunity. *Nat Immunol* **13**, 214-222 (2012).
13. Zhao, H. et al. A novel peptide with potent and broad-spectrum antiviral activities against multiple respiratory viruses. *Sci Rep* **6**, 22008 (2016).
14. Zhao, H. et al. Dual-functional peptide with defective interfering genes effectively protects mice against avian and seasonal influenza. *Nat Commun* **9**, 2358 (2018).
15. Yu, et al. A peptide-based viral inactivator inhibits Zika virus infection in pregnant mice and fetuses. *Nat Commun* **8**, 15672 (2017).
16. Lu, L. et al. Structure-based discovery of Middle East respiratory syndrome coronavirus fusion *Nat Commun* **5**, 3067 (2014).
17. Swanson, M.D. et al. Engineering a therapeutic lectin by uncoupling mitogenicity from antiviral *Cell* **163**, 746-758 (2015).
18. Leikina, E. et al. Carbohydrate-binding molecules inhibit viral fusion and entry by crosslinking membrane glycoproteins. *Nat Immunol* **6**, 995-1001 (2005).
19. Sample, C.J. et al. A mastoparan-derived peptide has broad-spectrum antiviral activity against enveloped viruses. *Peptides* **48**, 96-105 (2013).
20. Li, Q. et al. Virucidal activity of a scorpion venom peptide variant mucroporin-M1 against measles, SARS-CoV and influenza H5N1 viruses. *Peptides* **32**, 1518-1525 (2011).

21. Li, F. et al. A scorpion venom peptide Ev37 restricts viral late entry by alkalizing acidic organelles. *J Biol Chem* **294**, 182-194 (2019).
22. Smith, J.G. & Nemerow, G.R. Mechanism of adenovirus neutralization by Human alpha-defensins. *Cell Host Microbe* **3**, 11-19 (2008).
23. Brice, D.C. & Diamond, G. Antiviral Activities of Human Host Defense Peptides. *Curr Med Chem* (2019).
24. Klotman, M.E. & Chang, T.L. Defensins in innate antiviral immunity. *Nat Rev Immunol* **6**, 447-456 (2006).
25. Liu, S. et al. Different from the HIV fusion inhibitor C34, the anti-HIV drug Fuzeon (T-20) inhibits HIV-1 entry by targeting multiple sites in gp41 and gp120. *J Biol Chem* **280**, 11259-11273 (2005).
26. Gomes, B. et al. Designing improved active peptides for therapeutic approaches against infectious diseases. *Biotechnol Adv* **36**, 415-429 (2018).
27. Huotari, J. & Helenius, A. Endosome maturation. *EMBO J* **30**, 3481-3500 (2011).
28. Moscona, A. Entry of parainfluenza virus into cells as a target for interrupting childhood respiratory disease. *J Clin Invest* **115**, 1688-1698 (2005).
29. Hayden, F.G. et al. Baloxavir Marboxil for Uncomplicated Influenza in Adults and Adolescents. *N Engl J Med* **379**, 913-923 (2018).
30. Tan, Y.W., Yam, W.K., Sun, J. & Chu, J.J.H. An evaluation of Chloroquine as a broad-acting antiviral against Hand, Foot and Mouth Disease. *Antiviral Res* **149**, 143-149 (2018).
31. Li, C. et al. Chloroquine, a FDA-approved Drug, Prevents Zika Virus Infection and its Associated Congenital Microcephaly in Mice. *EBioMedicine* **24**, 189-194 (2017).
32. Wang, M. et al. Remdesivir and chloroquine effectively inhibit the recently emerged novel coronavirus (2019-nCoV) in vitro. *Cell Res* (2020).
33. Jurgeit, A. et al. Niclosamide is a proton carrier and targets acidic endosomes with broad antiviral effects. *PLoS Pathog* **8**, e1002976 (2012).
34. Kao, J.C. et al. The antiparasitic drug niclosamide inhibits dengue virus infection by interfering with endosomal acidification independent of mTOR. *PLoS Negl Trop Dis* **12**, e0006715 (2018).
35. Falzarano, D. et al. Lack of protection against ebola virus from chloroquine in mice and *Emerg Infect Dis* **21**, 1065-1067 (2015).
36. Paton, N.I. et al. Chloroquine for influenza prevention: a randomised, double-blind, placebo controlled trial. *Lancet Infect Dis* **11**, 677-683 (2011).
37. Seppala, et al. Flexible Structure of Peptide-Bound Filamin A Mechanosensor Domain Pair 20-21. *PLoS One* **10**, e0136969 (2015).
38. Nakano, S. et al. Structural and computational analysis of peptide recognition mechanism of class-C type penicillin binding protein, alkaline D-peptidase from Bacillus cereus DF4-B. *Sci Rep* **5**, 13836 (2015).

39. Hammen, P.K., Waltner, M., Hahnemann, B., Heard, T.S. & Weiner, H. The role of positive charges and structural segments in the presequence of rat liver aldehyde dehydrogenase in import into mitochondria. *J Biol Chem* **271**, 21041-21048 (1996).
40. Michen, B. & Graule, T. Isoelectric points of viruses. *J Appl Microbiol* **109**, 388-397 (2010).
41. Chandrababu, K.B., Ho, B. & Yang, D. Structure, dynamics, and activity of an all-cysteine mutated human beta defensin-3 peptide analogue. *Biochemistry* **48**, 6052-6061 (2009).
42. Liu, S. et al. Linear analogues of human beta-defensin 3: concepts for design of antimicrobial peptides with reduced cytotoxicity to mammalian cells. *Chembiochem* **9**, 964-973 (2008).
43. To, K.K. et al. Consistent detection of 2019 novel coronavirus in saliva. *Clin Infect Dis* (2020).
44. To, K.K. et al. Pulmonary and extrapulmonary complications of human rhinovirus infection in critically ill patients. *J Clin Virol* **77**, 85-91 (2016).
45. Zheng, B.J. et al. Delayed antiviral plus immunomodulator treatment still reduces mortality in mice infected by high inoculum of influenza A/H5N1 *Proc Natl Acad Sci U S A* **105**, 8091-8096 (2008).
46. Skinner, S.P. et al. CcpNmr AnalysisAssign: a flexible platform for integrated NMR analysis. *J Biomol NMR* **66**, 111-124 (2016).
47. Cheung, M.S., Maguire, M.L., Stevens, T.J. & Broadhurst, R.W. DANGLE: A Bayesian inferential method for predicting protein backbone dihedral angles and secondary structure. *J Magn Reson* **202**, 223-233 (2010).
48. Rieping, W. et al. ARIA2: automated NOE assignment and data integration in NMR structure *Bioinformatics* **23**, 381-382 (2007).
49. Laskowski, R.A., Rullmannn, J.A., MacArthur, M.W., Kaptein, R. & Thornton, J.M. AQUA and PROCHECK- NMR: programs for checking the quality of protein structures solved by NMR. *J Biomol NMR* **8**, 477-486 (1996).
50. Pettersen, E.F. et al. UCSF Chimera--a visualization system for exploratory research and analysis. *J Comput Chem* **25**, 1605-1612 (2004).

Figures

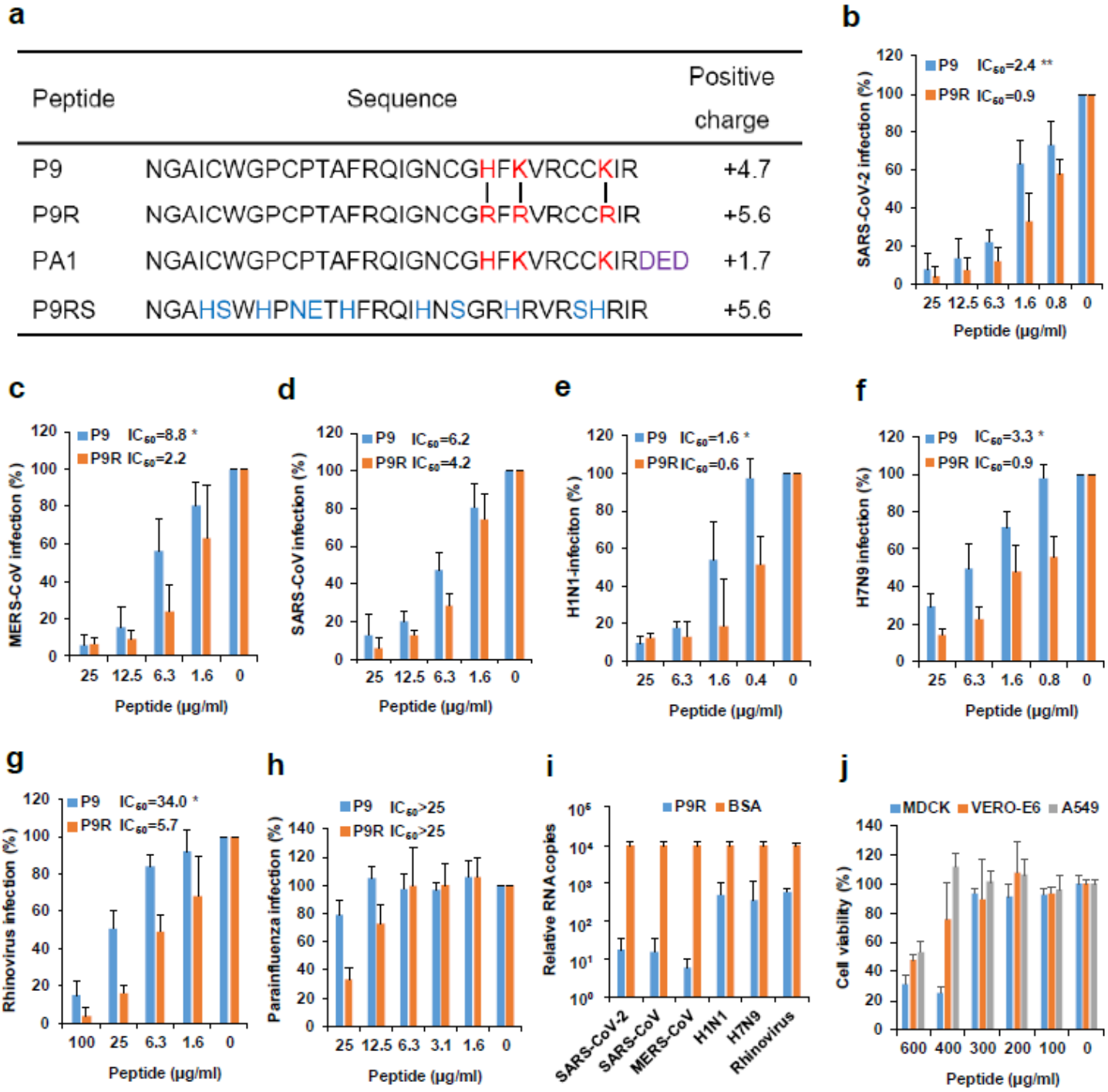

Figure 1

P9R could broadly inhibit enveloped and non-enveloped virus replication. (a) peptide sequences and positive charge analyzed by PepCalc of InnovaGen. (b-h) P9R could inhibit viral replication of 2019 new coronavirus (SARS-CoV-2), MERS-CoV, SARS-CoV, H1N1 virus, H7N9 virus, rhinovirus, and parainfluenza 3 virus in cells. Viruses were premixed with different concentrations of P9R or P9 and then infected cells. The antiviral efficiency was evaluated by plaque reduction assay. Infection (%) was calculated by the plaque number of virus treated with peptides being divided by the plaque number of virus treated by BSA.

(i) The potent antiviral activities of P9R against viruses by measuring the viral RNA copies in supernatants at 24h post infection when viruses were treated by P9R or BSA (50-100 μg ml-1). (j) Cytotoxicity of P9R in MDCK, Vero E6 and A549 cells. * indicates P<0.05 and ** indicates P<0.01 when IC50 of P9R compared with that of P9. P values were calculated by the two-tailed Student's t test. Data are presented as mean ±SD from at least three independent experiments.

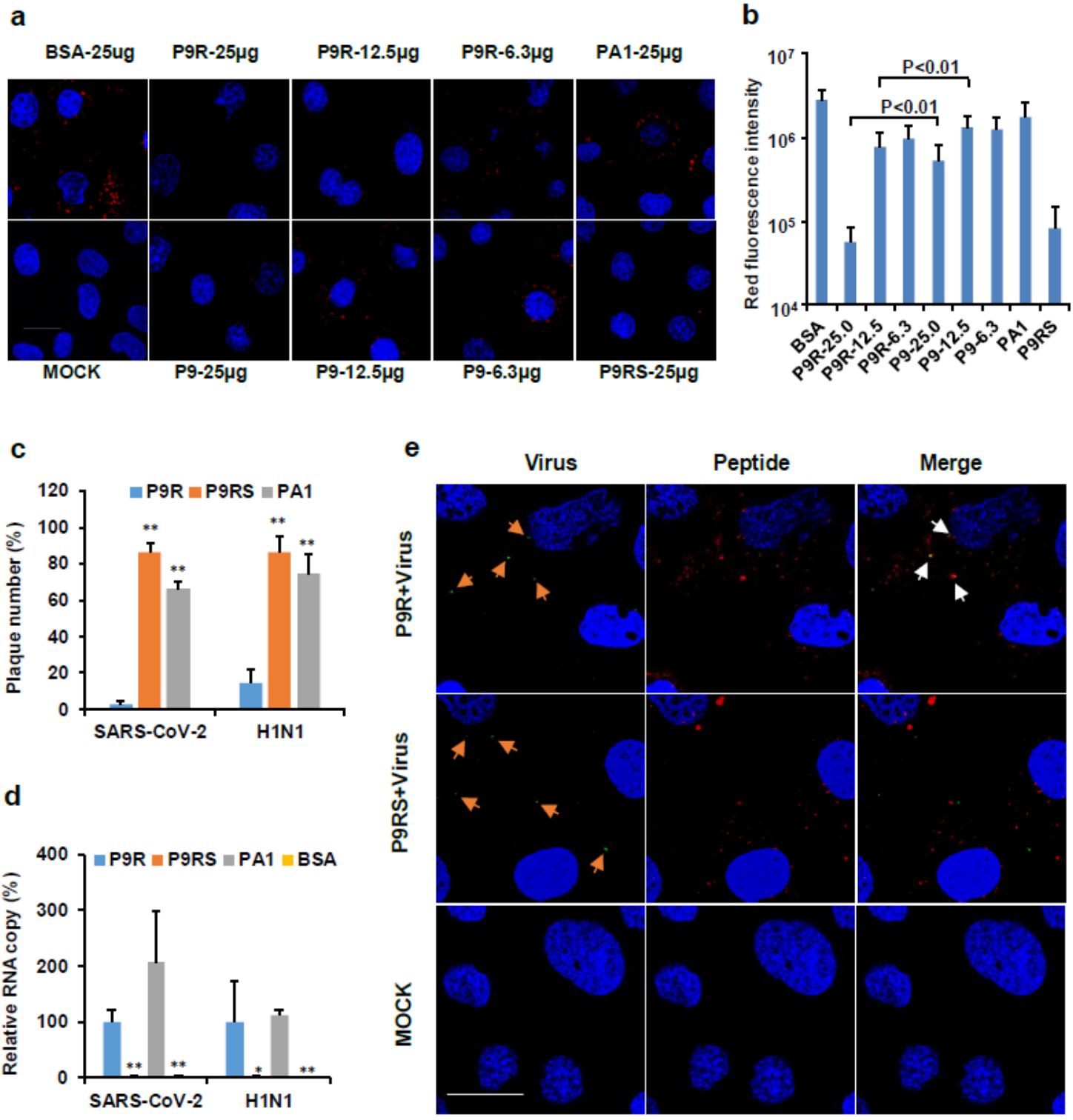

Figure 2

The enhanced antiviral mechanism of P9R. (a) P9R more efficiently blocked the endosomal acidification than that of P9. MDCK cells were treated by peptide and low pH indicator pHrodoTM dextran. Red dots (pHrodoTM dextran) indicated low pH in endosomes. Blue color indicates nuclei. Live cell images were taken by confocal microscope (original magnification 400 ×, scale bar = 20 μm). (b) The quantification of red fluorescence of endosomal acidification in MDCK cells treated by peptides. The red fluorescence intensity was calculated from 10 random microscope fields. (c) Antiviral activities of 25 μg ml-1 of P9R, P9RS, and PA1 against SARS-CoV-2 and A(H1N1)pdm09 virus were measured by plaque reduction assay. Plaque number (%) of peptide-treated virus was normalized to BSA-treated virus. (d) P9R and PA1 could bind to SARS-CoV-2 and A(H1N1)pdm09 virus. Viruses binding peptides were detected by ELISA and RT-qPCR. ** indicates $P<0.01$ when compared with P9R. P values were calculated by the two-tailed Student's t test. (e) P9R could more efficiently bind to virus in infected cells. Fluorescence labeled virus (green) was pretreated by TAMRA-labeled P9R (red) or TAMRA-labeled P9RS (red) for 1h. MDCK cells were infected with the treated virus. Images were taken by confocal microscope (scale bar = 20 μm). Orange arrows indicated viral particles. White arrows indicated P9R binding to virus. P9RS did not bind to virus.

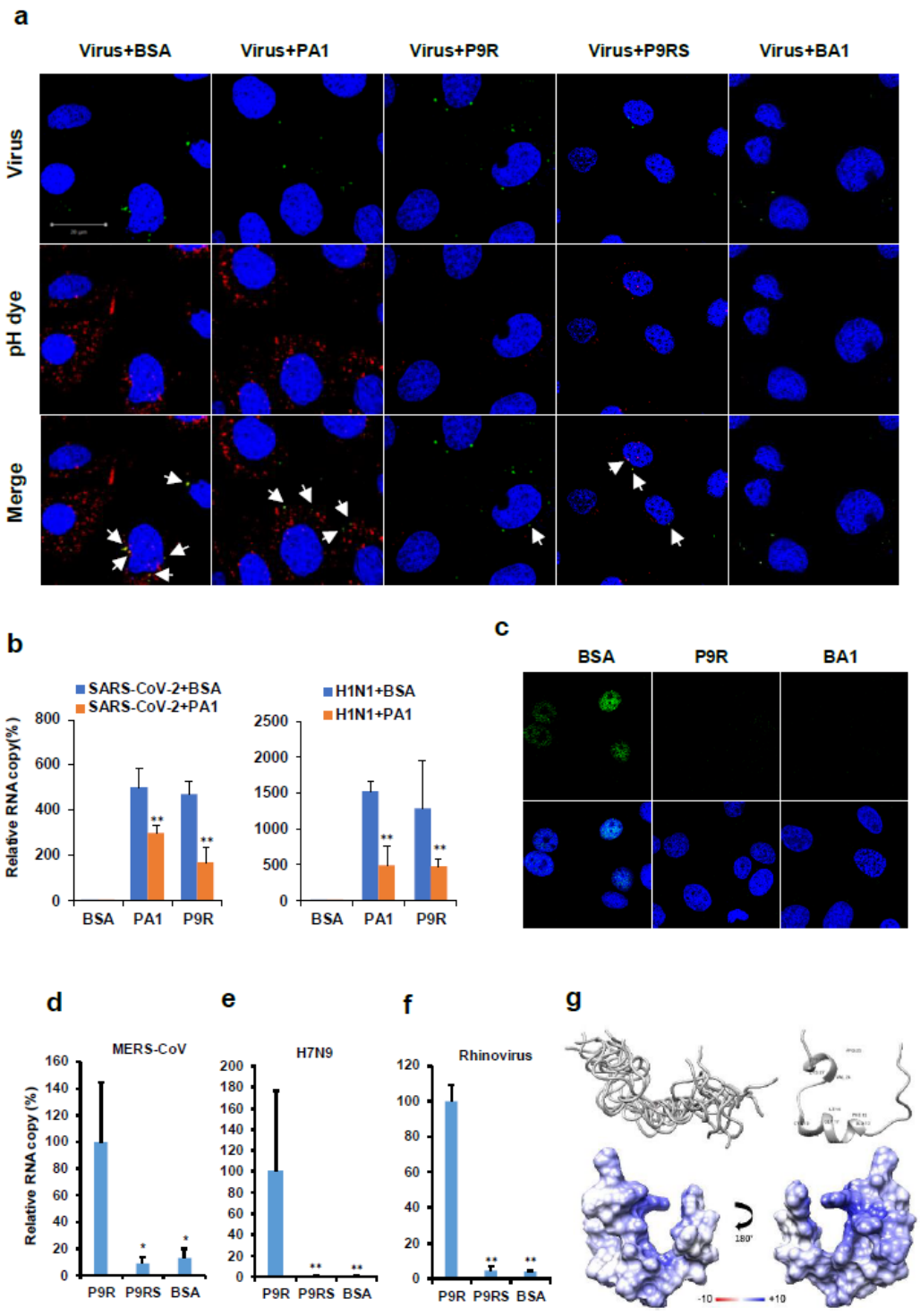

Figure 3

P9R could efficiently inhibit virus-host endosome acidification through directly binding to viruses. (a) Fluorescence labeled virus (green) was pretreated with indicated peptides (25 μg ml-1) or bafilomycin A1 (BA1). MDCK cells were infected with the treated H1N1-virus and low pH sensitive dye (red) was added to cells. Live cell images were taken by confocal microscope. (original magnification ×400, scale bar =20 μm). Red dot indicated the endosomal acidification. Nuclei was stained as blue. White arrows indicated

the colocalization of virus and endosomal acidification. (b) P9R binding to SARS-CoV-2 and A(H1N1)pdm09 could be reduced by PA1. Virus was pretreated by PA1 or BSA, and then the treated virus binding to the indicated peptides were measured by RT-qPCR. ** indicates P<0.01 when compared virus treated by BSA. (c) P9R could inhibit viral RNP release into nuclei. H1N1 virus was pretreated by BSA, P9R or bafilomycin A1 (BA1), and then MDCK cells were infected with the treated virus. Images of viral NP (green) and cell nuclei (blue) were taken at 3.5 h post infection. (d-g) P9R could broadly bind to MERS-CoV, H7N9 virus, and rhinovirus. The relative RNA copy of virus binding to peptides was normalized to the virus binding to P9R. * indicates P<0.05. ** indicates the P<0.01 when compared with P9R. P values were calculated by the two-tailed Student's t test. (h) Top left: top 10 water-refined structures of P9R generated by ARIA displayed as backbone traces, showing an overall flexible structure. Top right: representative NMR structure of P9R displayed as ribbon plot showing the formation of some helix patches. Bottom: surface charge plot of the representative NMR structure of above P9R showing largely positively charged peptide surface.

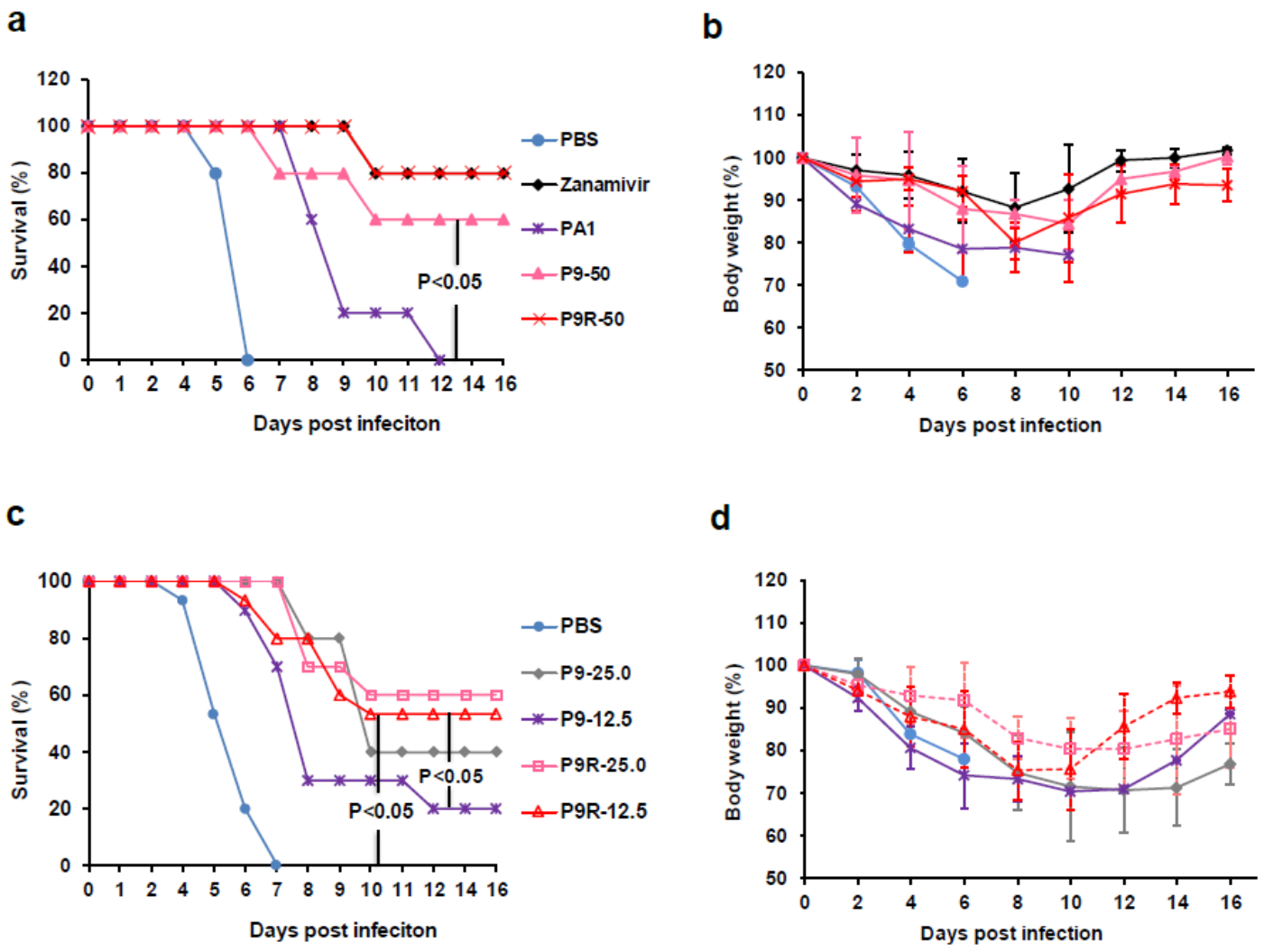

Figure 4

The therapeutic protection of P9R on A(H1N1) infected mice. (a) P9R (50 μg/dose) could provide similar therapeutic efficacy on mice infected by A(H1N1) virus as that of zanamivir (Zana, 50 μg/dose). PBS, zanamivir, PA1, P9R, or P9 were intranasally inoculated to mice at 6 h post infection and two more doses were administrated to mice in the following one day. Five mice in each group were included. (b) The body weight change of infected mice corresponding to (a). (c) Low doses of P9R could more efficiently protect mice infected by A(H1N1)pdm09 virus than that of P9. PBS (n=10), P9- 25 (25.0 μg/dose, n=5), P9-12.5 (12.5 μg/dose, n=5), P9R-25 (25.0 μg/dose, n=10), and P9R-12.5 (12.5 μg/dose, n=10) were intranasally inoculated to mice at 6 h post infection and two more doses were administrated to mice in the following one day. (d) The body weight change of infected mice corresponding to (c). P values were calculated by Gehan-Breslow-Wilcoxon test.

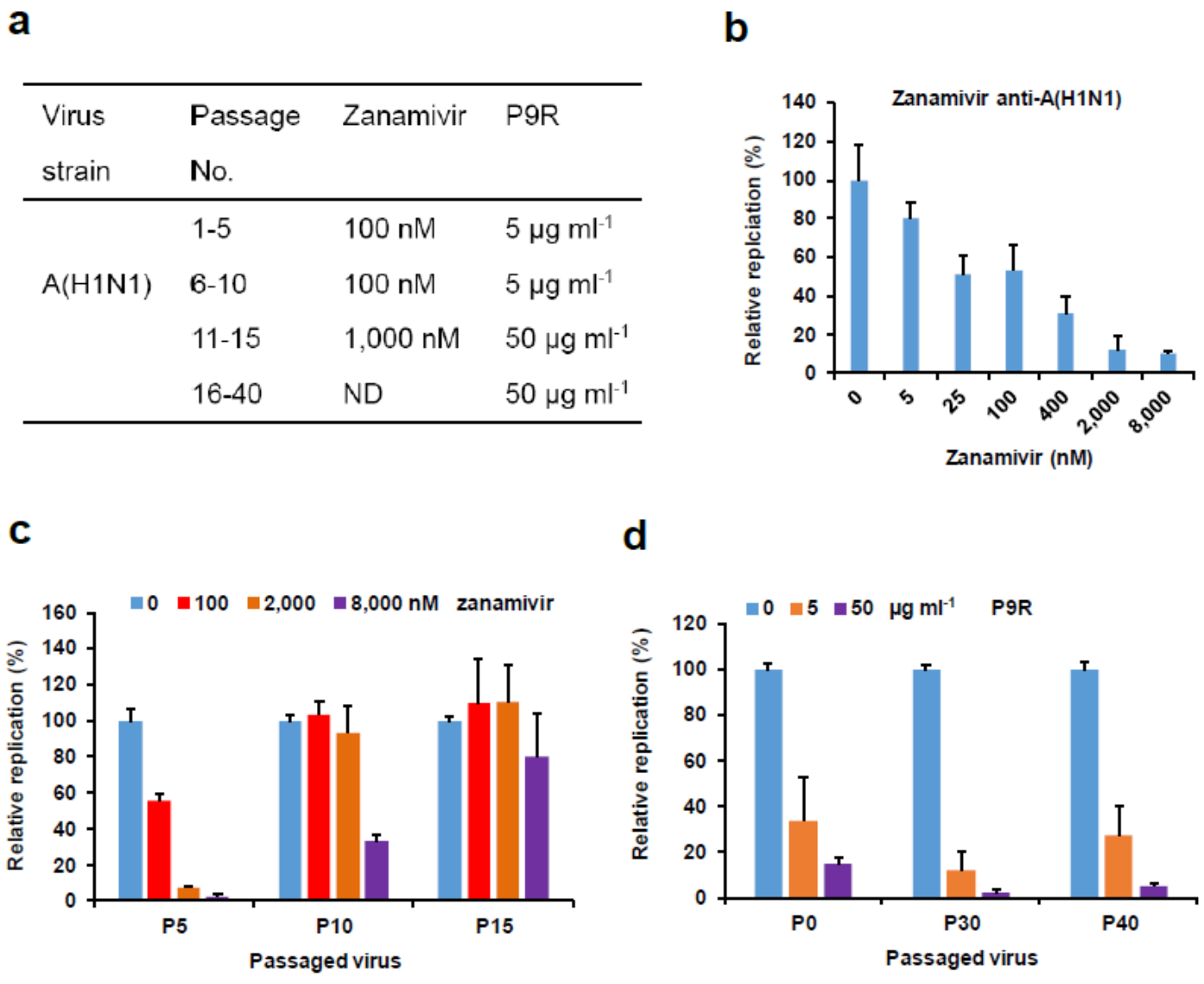

Figure 5

P9R showed low possibility to cause drug-resistance virus. (a) The procedure of drug- resistance assay for zanamivir and P9R. A(H1N1) virus was passaged in the presence of indicated concentrations of

zanamivir and P9R. ND, not detected because the high resistant H1N1 virus against zanamivir was generated before P16. (b) Zanamivir inhibited parent A(H1N1) virus (P0). The IC50 of zanamivir against parent H1N1 was 35 nM. (c) The antiviral efficiency of zanamivir against passaged A(H1N1) virus in the presence of zanamivir. (d) The antiviral efficiency of P9R against passaged A(H1N1) virus in the presence of P9R. Passaged viruses were premixed with zanamivir (nM) or P9R (μg ml-1) for infection. Supernatants were collected at 24 h post infection. Viral titers in the supernatants were determined by RT-qPCR. The relative replication (%) was normalized to the corresponding passaged viruses without treatment. Data are presented as mean ±SD of three independent experiments.

Supplementary Files

This is a list of supplementary files associated with this preprint. Click to download.

- Supplementalinformation.pdf